SYNTHESIS, CHARACTERIZATION AND DFT THEORETICAL STUDIES OF METFORMIN WITH GLYCINE MIXED LIGAND AND THEIR COMPLEXES WITH URANYL IONS.

Darwish, M.M.* ; S.A. Abdel-Latif
and A.A. Mohamed
Chemistry Department, Faculty of Science, Helwan University, Cairo, Egypt
*E-mail: magdydarwish754@gmail.com

ABSTRACT

The Complexes of UO_2 (II) with Metformin ligand (1,1-dimethyl biguanide) (Met)and Glycine (Gly) as mixed ligand (Aminoacetic acid) have been prepared and characterized using different techniques. Theoretical studies (density functional theory, DFT) were also carried out to support the corresponding experimental results. Computational calculations were achieved using a level of theory DFT/GEN for the metal. The nature of the interaction between the metal ions & the ligand, molecular stability, and bond strengths have been studied using DFT calculations employing natural bond orbital (NBO) analysis. The regioselectivity of the reaction was supported by theoretical calculations at the DFT level. The optimized molecular structure and natural bond orbital (NBO) have been performed by density functional theory (DFT) using the B3LYP method with the 6-311++G(d,p) basis set for the ligands.

Key Words: Uranyl complexes, Metformin, Glycine, DFT, and NBO.

INTRODUCTION

Metformin was approved in the United Kingdom in 1958 and the United States in 1995.Metformin has been converted into a more widely used drug for the treatment of type 2 diabetes (DM2) at doses between 500 and 2500 mg/day **(Scarpello and Howlett 2008)**. According to the guidelines of the American Diabetes Association/European Association for the study of diabetes, metformin is the first-line therapy for T2DM patients **(Inzucchi *et al.,* 2012)**. Metformin lowers blood glucose concentrations without causing hypoglycemia by reducing intestinal glucose uptake, improving peripheral glucose uptake, lowering fasting plasma insulin levels, and increasing insulin sensitivity **(Grzybowska *et al.,* 2011)**. Additionally, metformin can reduce gluconeogenesis by triggering AMP-activated protein kinase (AMPK) **(Matthaei and Greten , 1991)**. Recent research suggests that metformin may have

additional benefits outside decreasing blood sugar, including anticancer, antiaging, cardiovascular protective, neuroprotective, and polycystic ovary syndrome (PCOS) therapy options (**Wang** *et al.,* **2017**). Due to the corresponding drug metal complexes' improved biological activity, metal complexes preparation have been the focus (**Bentefrit** *et al.,* **1997**). It was discovered that the platinum (IV) complex exhibits anticancer activity, while the vanadyl complex with metformin exhibits potential synergistic insulin mimics (**Shahabadi and Heidari, 2012**). Looking at the significance of metformin, the other metformin complexes, such as complexation with chromium, are thought to be the most commonly prescribed antidiabetic medication worldwide (**Krishan** *et al.,* **2012**). Additionally, studies of metformin complexes such as Co (II), Zn (II), and Pt (II) complexes have interesting thermal behavior in addition to having an antibacterial activity (**Viossat,** *et al.,* **1995 ; Lemoine,** *et al.,***1996 ; Zhu,** *et al.,* **2002a and Olar,** *et al.,* **2005**. The metformin ligand's metal complexes are typically cationic, and its brightly coloured chelate changes depending on the type of metal ion, its oxidation state, the number of ligands present in the complex, and these factors together serve as chelating agents (**Scarpello and Howlett 2008**). Numerous transition elements, in particular copper (II), nickel (II), cobalt (II), and platinum (II), interact with metformin to generate the compounds [PtCl (MF)(DMSO)]Cl, [PtCl$_4$(MF)(DMSO)], [Co (MF.HCl) (Cl)$_2$], [CuCl$_2$ (MF)$_2$], and [Cu(MF)$_2$]. Zn(MF.HCl) Cl$_2$.2H$_2$O, and Ni(MF)$_2$ (**Viossat,** *et al.,* **1995 ; Lemoine,** *et al.,***1996 ; Bentefrit** *et al.,* **1997 and Zhu,** *et al.,* **2002b**). It contains two donor centers for amino groups and one donor center for each of the primary, secondary, and tertiary amino groups. Water readily dissolves metformin hydrochloride, whereas acetone, ether, and chloroform are essentially insoluble. 2.8 and 11.51 are the pKa values for metformin. Its melting point is 222-226 ^{o}C (**Refat,** *et al.,* **2015**).

In this study, metformin uranyl complexes were synthesized and characterized, and the structures of complexes will be investigated using several techniques. The analysis of natural bond orbital (NBO) on complexes is reported, The different quantum chemical parameters such as bond lengths, bond angles, electronic dipole moment (μ) as well as first-order hyperpolarizability (β), energy minimization analyses, molecular orbitals (MOs), quantum chemical parameters, HOMO-LUMO energy gap (Eg), absolute electronegativities (χ), absolute hardness (η), absolute softness (σ), chemical potentials (P), global softness (S), global

electrophilicity (ω), and additional electronic charge (ΔNmax) have been computed at the DFT-B3LYP/GEN level of calculation. A comparison of computed structural and spectroscopic data with reported experimental results has been done.

EXPERIMENTAL

1. Chemicals and reagents.

All chemicals and reagents used in the synthesis of the UO_2-Met and UO_2-Met-Gly complexes were of analytical grade and were used without further purification. Hydrated uranyl sulfate ($UO_2SO_4.3\frac{1}{2}H_2O$) was provided by Alfa-Aesar (Germany) and Glycine (Gly) by NICE (India). Metformin (Met) and ethanol were supplied by Sigma-Aldrich (Germany).

2. Instruments.

UO_2-Met and UO_2-Met-Gly complexes were characterized using various techniques. Elemental analysis (C, H, N, and S) was performed using an automatic analyzer (Vario ELIII-Elementer, Germany). UO_2-Met complexes (1:1, 1:2 and 1:1:1) were investigated using a Fourier transform infrared (FT-IR) spectrometer [FTIR-JASCO 3600 (400-4000 cm^{-1})] with KBr discs at room temperature. ^{1}H NMR spectra in DMSO-d6 were developed using a Gemini 300 MHz NMR spectrometer (ECA 500 II, JEOL, Japan). The mass spectrometry of the UO_2-Met and UO_2-Met-Gly complexes were recorded using Thermo Scientific, ISQ Single Quadrupole MS. Thermogravimetric analysis (TGA) evaluated the thermal stability of the UO_2-Met and UO_2-Met-Gly complexes was done using an SDTQ600 analyzer at 10 °C min under nitrogen atmosphere.

3. Synthesis.

3.1. Synthesis of UO_2-Met (1:1) complex.

For the synthesis of UO_2-Met (1:1) complex, a 1:1 molar ratio reflux method was employed using Metformin (Met) and hydrated uranyl sulphate ($UO_2SO_4.3\frac{1}{2}H_2O$) as shown in Fig 1, 0.1656 g (1.0 mmol) of Metformin was completely dissolved in hot ethanol with vigorous stirring (solution-A), then 0.429 g (1.0 mmol) of $USO_4.3\frac{1}{2}H_2O$ was dissolved with stirring (solution-B). Then, solution-B was added dropwise to the above mixture (solution-A) with stirring. Mixtures (A) and (B) were transferred to a round-bottomed flask with an ammonia-water solution (1:10) to increase the reaction rate and to be able to modify the pH of the solution (pH= 7-7.5) and prevent hydrolysis, then brought to reflux for 4

hours. Then the UO$_2$-Met complex (1:1) was obtained, which was filtered, washed with hot ethanol, and dried under vacuum at 50°C.
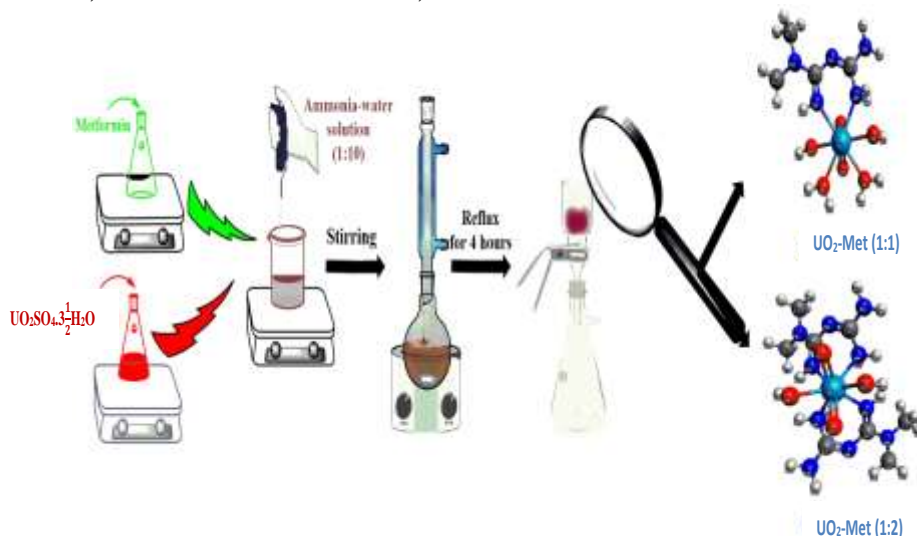
Fig 1. Schematic preparation of UO$_2$-Met (1:1 and 1:2)

3.2. Synthesis of UO$_2$-Met (1:2) complex.

A reflux method was adopted for the synthesis of UO$_2$-Met (1:2) complex using Metformin hydrochloride (C$_4$H$_{12}$N$_5$Cl), and hydrated uranyl sulphate (UO$_2$SO$_4$.3$\frac{1}{2}$H$_2$O) with molar ratios of 1:2. The preparation steps are similar to that of UO$_2$-Met (1:1) but with a higher ratio of Metformin to uranyl sulphate ratio (Fig 1).

3.3. Synthesis of UO$_2$-Met-Gly (1:1:1) complex.

The regression method was used to synthesize UO$_2$-Met-Gly (1:1:1) complex as shown in Fig 1. 0.1656 g (1.0 mmol) of Metformin was completely dissolved in hot ethanol with vigorous stirring (solution A), then 0.429 g (1.0 mmol) USO$_4$.3$\frac{1}{2}$H$_2$O was dissolved in hot ethanol with stirring solute-B) . 0.7507 g (1.0 mmol) of Glycine was also dissolved in hot ethanol with vigorous stirring (solution C). Then solution B is added dropwise to solution (A) while stirring. Mixes (A) and (B) were transferred to a round bottom flask, then solution (C) was added to the mixture (A, B) with the addition of ammonia solution in the ratio (1:10) to adjust the pH of the solution (pH= 7-7.5), then reflux for 4 hours. The UO$_2$-Met-Gly complex (1:1:1) was then obtained, which was filtered, washed (hot ethanol), and dried under reduced pressure at 50 °C.

Fig 2. Schematic preparation of UO_2-Met-Gly complex (1:1:1)

4. Computational details.

Due to the absence of single crystal X-ray structure analysis and to attain the molecular conformation of compounds Metformin, Glycine, UO_2-Met (1:1), UO_2-Met (1:2), and UO_2-Met-Gly (1:1:1), energy minimization analyses were done by means of Gaussian-09W software package (**Frisch *et al.,* 2010**), with the B3LYP exchange correlation functional approach. The basis set 6-311G** was applied for C, H and N atoms and SDD for UO_2(II). Without any symmetry constraints, the geometry of the investigated systems was totally optimized in gas-phase. Gauss View 5 software (**Dennington *et al.,* 2009**) was used to create figures of molecular orbitals (MOs) by visualization of the structures. The quantum chemical parameters of the studied compounds were gained from calculations as energies of the lowest unoccupied molecular orbital (E_{LUMO}), the highest occupied molecular orbital (E_{HOMO}) (Fig 1. (Eg): HOMO-LUMO energy gap, (χ): Absolute electronegativities, (η): Absolute hardness, (σ): Absolute softness, (P): Chemical potentials, (S): Global softness, (ω): Global electrophilicity, (ΔNmax): Additional electronic charge, these parameters were calculated using the following equations (1-8):

$$Eg = E_{LUMO} - E_{HOMO} \qquad (1)$$

$$\chi = \frac{-E_{LUMO} - E_{HOMO}}{2} \qquad (2)$$

$$\eta = \frac{E_{LUMO} - E_{HOMO}}{2} \qquad (3)$$

$$\sigma = \frac{1}{\eta} \qquad (4)$$

$$p = -\chi \qquad (5)$$

$$S = \frac{1}{2\eta} \qquad\qquad (6)$$

$$\omega = \frac{P^2}{2\eta} \qquad\qquad (7)$$

$$\Delta Nmax. = \frac{-P}{\eta} \qquad\qquad (8)$$

The mean polarizability ($<\alpha>$), polarizability anisotropy ($\Delta\alpha$), mean first-order hyperpolarizability ($<\beta>$), and total static dipole-moment (μ) were estimated using the x, y, and z components (**Avci *et al.*, 2010 and Avci, 2011**).

RESULTS AND DISCUSSION

FTIR spectra were obtained for UO_2-Met (1:1), UO_2-Met (1:2), and UO_2-Met-Gly (1:1:1) complexes (Fig). Pure Metformin spectrum demonstrated characteristic sharp peaks at 3370, 3295, and 1661 cm^{-1} corresponding to NH stretching of the amine group (expected site of complexation), NH stretching of the imido group, and C=N stretching. Also, the peaks at 1419, and 1558 cm^{-1} correspond to the C-H asymmetric of methyl CH_3 group and binding N-H bonds respectively (**Panda *et al.*, 2018 and Abd-El Hafeez *et al.*, 2022**). Pure glycine spectrum showed symmetric and asymmetric carboxyl group (–COO) frequencies at 1402 cm^{-1} (C=O) and 1582 cm^{-1}, The stretching of NH_2 shows a characteristic peak around 3400 cm^{-1}, The peaks of C-H appear in the range of 1200 cm^{-1} to 1300 cm^{-1} (**Chen *et al.*, 2021**).

UO_2-Met (1:1), UO_2-Met (1:2) spectra show peaks at 3544 cm^{-1} and 3328 cm^{-1} which attributed to the N-H stretching of the amine and imido groups respectively, that shifted from the pure peaks of that groups in the pristine Metformin. This shift revealed the inclusion of the nitrogen atoms of amine and an imido group of Metformin in the complexation with uranyl metal ions. The vibration of C=N in the prepared UO_2-Met (1:1), UO_2-Met (1:2) complexes shifted from 1661 to 1693 cm^{-1}. Also, the peaks of N-H binding, and asymmetric C-H of the methyl group shifted after complexation from 1419, and 1558 cm^{-1} to 1602, and 1489 cm^{-1} respectively. The peaks that appeared at lower wave number 767-601 cm^{-1} may be due to the (U←N) coordinate bond (**Mahmoud *et al.*, 2019**). UO_2-Met-Gly (1:1:1) spectrum showed a weak intensity peak at 1618 cm^{-1} that characteristic of glycine which shifted from 1582 cm^{-1} in the pristine glycine. The shift in the C=O position may be due to the inclusion of the complexation with uranyl metal ions. The appearance of peaks at 567 cm^{-1} may be attributed to the (U←O) coordinate bond (**Chen *et al.*, 2021**).
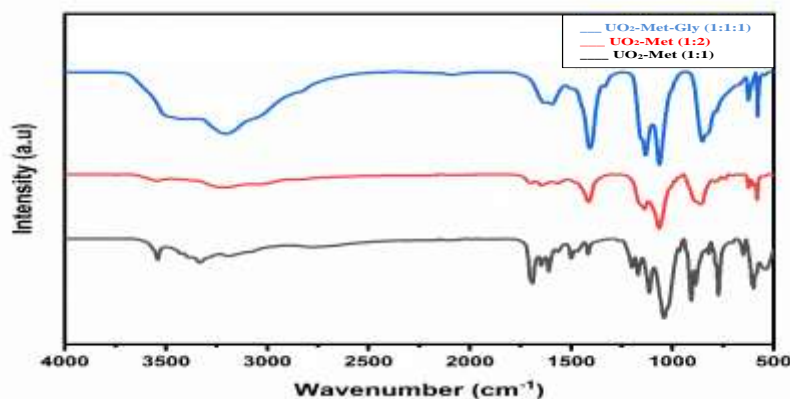
Fig 3. FTIR spectra of UO_2-Met (1:1), UO_2-Met (1:2), and UO_2-Met-Gly (1:1:1) complexes.

CHN analysis of UO_2-Met (1:1), UO_2-Met (1:2), and UO_2-Met-Gly (1:1:1) complexes were compared with theoretically calculated and represented in Table 1. The results are in excellent conformity with the proposed chemical formulae; $C_4H_{19}N_5O_6U$, $C_8H_{24}N_{10}O_4U$, and $_7H_{18}N_6O_6U$, respectively.

Table 1. Theoretically and experimentally elemental analysis of the UO2-Met (1:1), UO2-Met (1:2), and UO2-Met-Gly (1:1:1) complexes

Element	Theoretically calculated			Found CHN elemental analysis		
	UO_2-Met (1:1)	UO_2-Met (1:2)	UO_2-Met-Gly (1:1:1)	UO_2-Met (1:1)	UO_2-Met (1:2)	UO_2-Met-Gly (1:1:1)
C	10.23	10.81	10.30	9.94	10.47	10.17
H	3.762	5.40	3.43	3.62	5.23	3.37
N	14.92	15.76	18.02	14.67	15.62	17.94

The experimental ^{1}H NMR spectra of UO_2-Met (1:1), UO_2-Met (1:2), and UO_2-Met-Gly (1:1:1) complexes (Fig), UO_2-Met (1:1) showed signals at δ 2.4-2.8 ppm, the signal at 2.5 and the weak intense signal at 2.8 ppm were attributed to the presence of solvent water molecules, respectively (**Babij** *et al.,* **2016 and Heidari** *et al.,* **2017**). While the signal at 3-3.3 may be attributed to protons of the methyl group, the broad peak at 3.0, and 3.3 were attributed to H_2O and NH protons. The broadening may be due to the exchangeable ability of these acidic

protons which resulted in no coupling with its neighbor protons (**Robert et al., 2020**). The signals at 6.4 to 6.7 ppm may be attributed to the amine protons. Fig   shows the ^{1}HNMR spectrum of the UO$_2$-Met (1:2) complex., The spectrum shows similar signals to UO$_2$-Met (1:1) complex with a little variation in the peaks broadening and intensities.
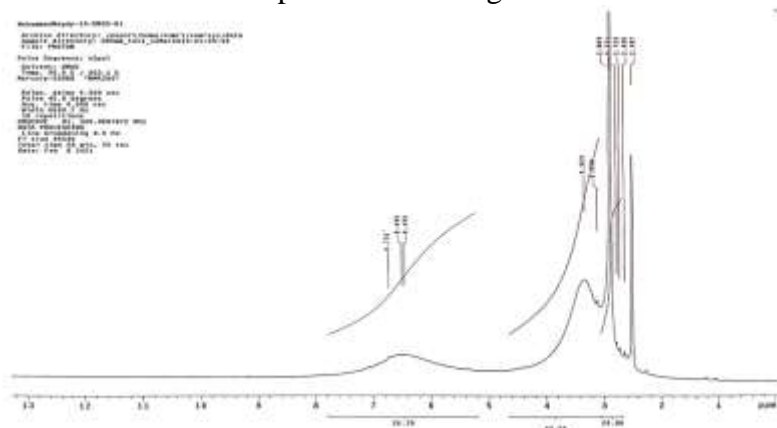
Fig 4. ^{1}H NMR spectrum of UO$_2$-Met (1:1) complex.
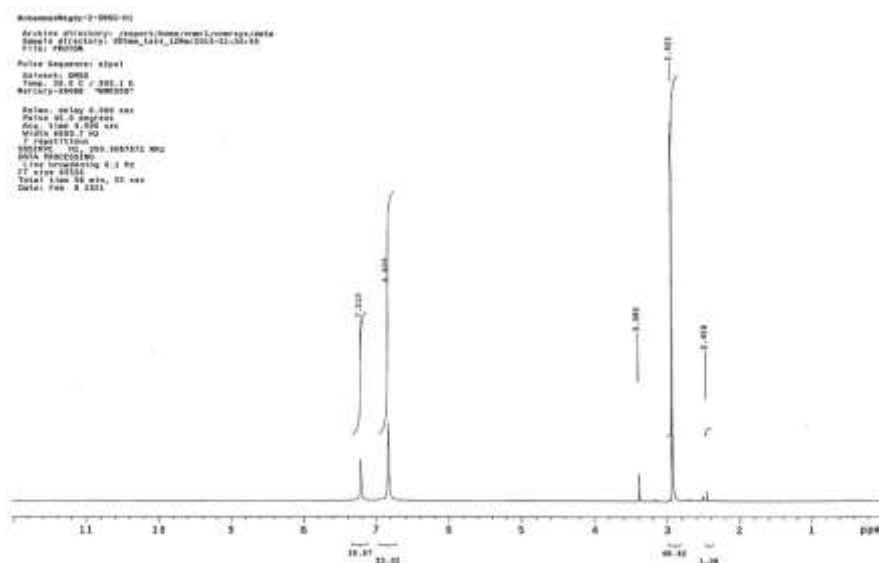
Fig 5. ^{1}H NMR spectrum of UO$_2$-Met (1:2) complex.

Fig -8) represent the mass spectra of UO$_2$-Met (1:1), UO$_2$-Met (1:2), and UO$_2$-Met-Gly (1:1:1) complexes, respectively. The molecular ion peaks were at 432, 652, and 523 m/z, respectively. The base peak for

UO_2-Met (1:1), UO_2-Met (1:2), and UO_2-Met-Gly (1:1:1) complexes appeared at 85, 120, and 69 m/z, respectively, which corresponds to the proposed structure of the three prepared complexes.
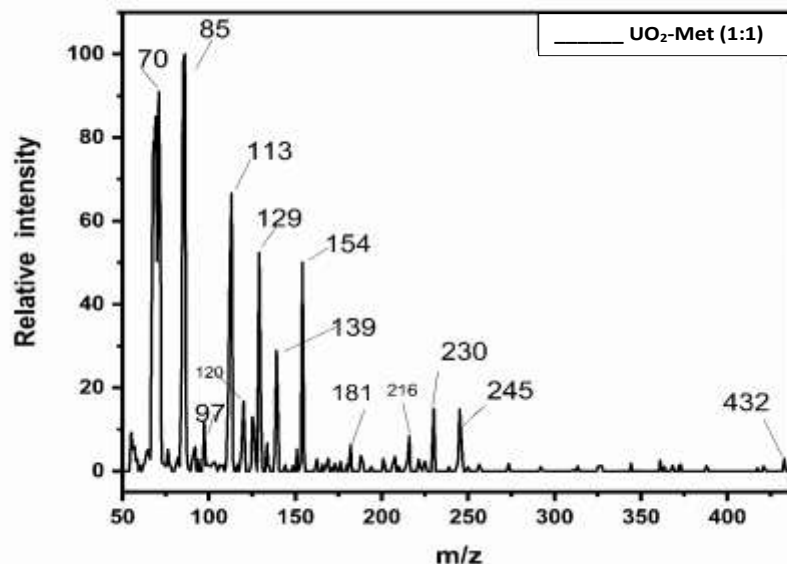
Fig 6. Mass spectrum of UO_2-Met (1:1) complex.
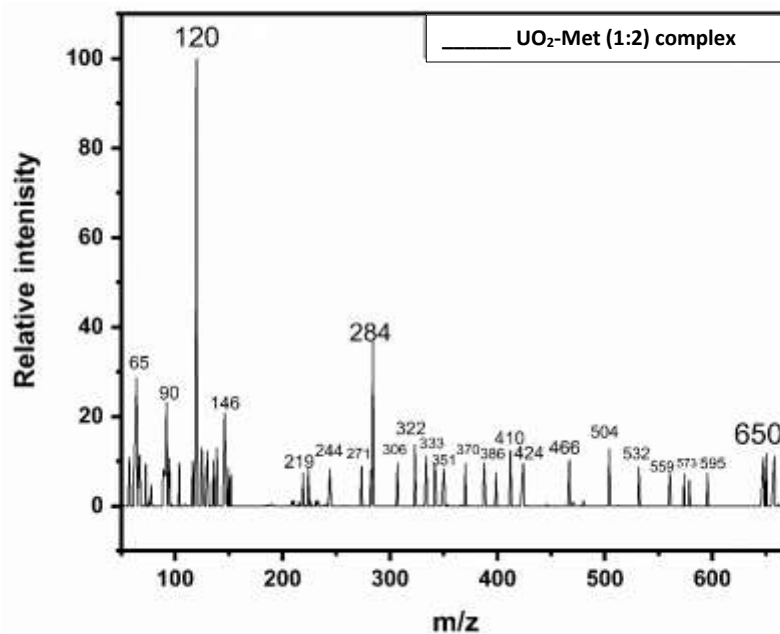
Fig 7. Mass spectrum of UO_2-Met (1:2) complex.
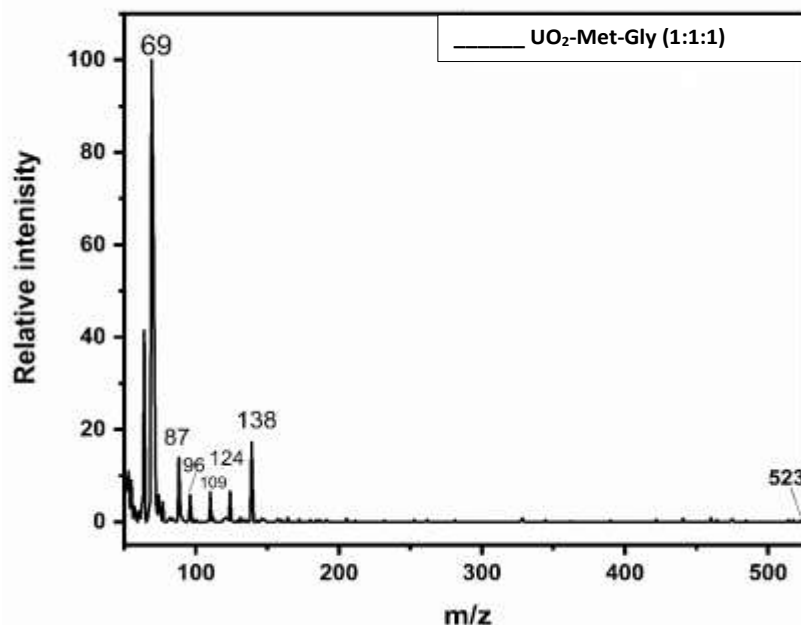
Fig 8. Mass spectrum of UO_2-Met-Gly (1:1:1) complex.

The thermal stability of the UO_2-Met (1:2) and UO_2-Met-Gly (1:1:1) complexes was tested under nitrogen atmosphere at 800°C/10°C per minute. Molecules of hydrated water are connected by a complex configuration and are located outside the coordination region formed around the central metal ion. Dehydration of this type of water occurs in the temperature range of 25-220°C, and the weight loss corresponds to one molecule of water. On the other hand, coordinated water molecules are removed at higher temperatures than hydrated water molecules. The consistency of water is usually in the temperature range of 100-316°C (**Abdel-Ghani and Sherif, 1989**). The organic portion of the complex may decompose in one or more steps with the potential to form another intermediate product. These intermediates may contain metal ions with some bonds (**Abdel-Latif *et al.*, 2007**). These intermediates can eventually be decomposed down into stable metal oxides. The thermogram indicates that the decomposition of the UO_2-Met (1:2) complex went through four steps. The first phase of weight loss (DTA, 132.22 °C) was about 4.028%, and raising the temperature up to 170 °C corresponds to the loss of one water molecule. The second stage of weight loss (DTA, 222.82 °C) was 5.719% when the temperature rises to about 268 °C, corresponding to the loss of coordinated water molecules. When the temperature was increased to 388 °C (step 3 (DTA, 368.66

°C)), this corresponds to the loss of coordinated water molecules, and the thermogram loses mass due to a decrease of 12.560% in the sample weight was shown. The intermediate species formed by raising the organic fraction temperature of the compound to 555 °C (stage IV (DTA, 458.55 °C)) and decomposition. The thermogram showed an 18.84% decrease in sample weight. At elevated temperatures, the analyzed UO_2-Met (1:2) complex exhibited a significant thermal stability of up to 800 °C with slight loss. The remaining residue was about 58.80% by weight, which persists until a constant load was reached where the metal oxide residue was formed.
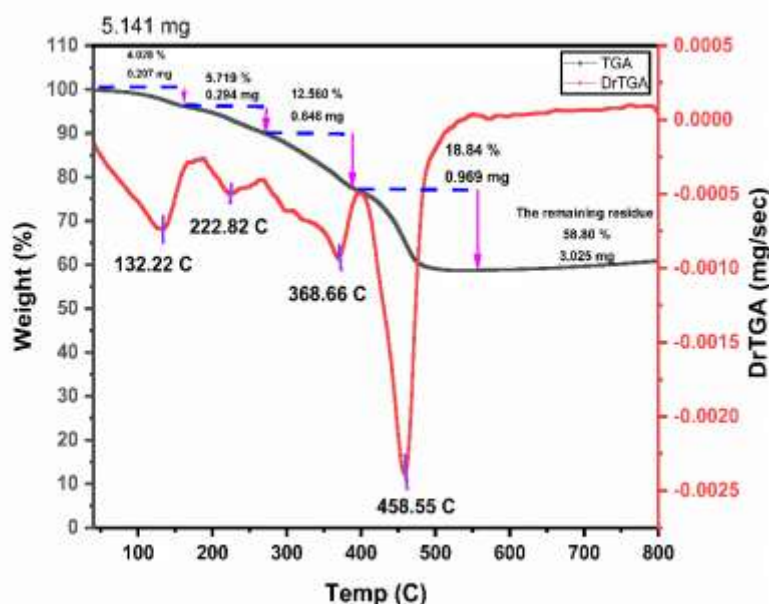
Fig 9. The thermogravimetric analysis (TGA-DTA) of UO_2-Met (1:2) complex

The thermogram shows that the decomposition of the UO_2-Met-Gly complex (1:1:1) went through four steps. The first stage (DTA, 61.36 °C) had a 4.45% weight loss with increasing temperature up to 144 °C, which corresponds to the loss of one hydrated water molecule. The second stage (DTA, 130.20 °C) had a 8.62% weight loss with the temperature rising to 285 °C, which corresponds to the loss of coordinated water molecules. With a further increase in temperature up to 362 °C (phase III (DTA, 345.11 °C)) corresponding to the loss of coordinated water molecules, the thermogram showed a weight loss of the sample of 4.05% caused by

the formation of intermediate species by fractional decomposition for the organic residue, the thermogram showed 11.23% sample weight loss upon increasing the temperature to 578 °C (Stage IV (DTA, 488.31 °C)). At higher temperature, the analyzed UO_2-Met-Gly complex (1:1:1) showed significant thermal stability up to 800 °C with slight loss. The remaining residue was 71.65% (metal-oxide).
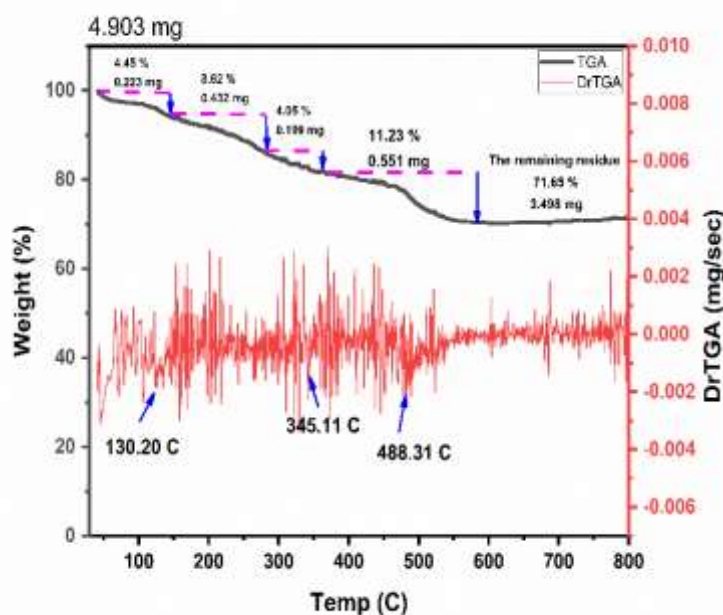
Fig 10. The thermogravimetric analysis (TGA-DTA) of UO_2-Met-Gly
        (1:1:1) complex

1. Theoretical studies

Different quantum chemical parameters such as, bond lengths, bond angles (Table 2), The values of the dihedral angles were far from 0° or 180° which confirm that the examined ligands and their complexes has a complete non-planar structure. Electronic dipole moment (μ) as well as first-order hyperpolarizability (β) were calculated using the DFT-B3LYP/6-311G** level of calculation for C, H, N, O and SDD for UO_2(II). Quantum mechanical calculations of geometries and energies were attained using the density functional theory with Becke's three-parameter exchange functional method, the Lee-Yang-Parr correlation

functional approach (B3LYP/DFT) combined with B3LYP/GEN level basis sets was used (Fig 1).

Metformin

Glycine

UO$_2$-Met (1:1)

UO$_2$-Met (1:2)
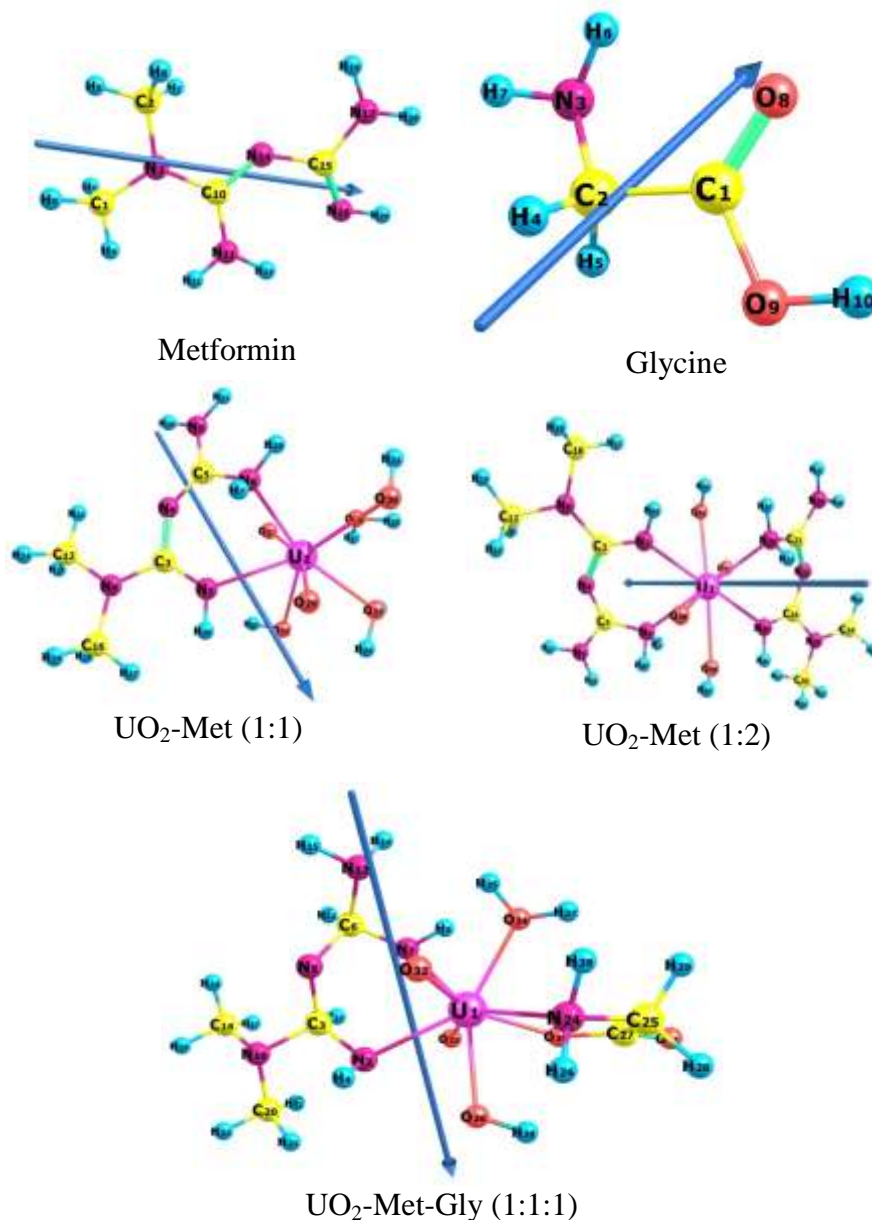
UO$_2$-Met-Gly (1:1:1)

Fig 11. Optimized geometry, numbering system, and vector of the dipole moment of Metformin, Glycine, UO$_2$-Met (1:1), UO$_2$-Met (1:2), and UO$_2$-Met-Gly (1:1:1) using B3LYP/6.311G** and B3LYP/ GEN level.

Table 2. Selected geometric bond lengths, bond angles and dihedral angles of the optimized Metformin, Glycine, UO$_2$-Met (1:1), UO$_2$-Met (1:2), and UO$_2$-Met-Gly (1:1:1) using B3LYP/GEN level.

Compound	Bond lengths (A)		Bond angles°		Dihedral angles°	
Metformin	C1-N5	1.457	C1-N3-C2	116.566	C1-N3-C10-N11	1.091
	N3-C2	1.456	C1-N3-C10	124.623	C1-N3-C10-N14	-178.281
	N3-C10	1.448	C10-N3-C3	118.811	C2-N3-C10-N11	-179.056
	N11-C10	1.434	N3-C10-N11	121.165	C2-N3-C10-N14	1.573
	N14-C10	1.303	N3-C10-N14	117.121	N11-C10-N14-C15	2.551
	N14-C15	1.431	N11-C10-N14	121.711	C10-N14-C15-N16	8.966
	C15-N16	1.284	C10-N14-C15	132.078	C10-N14-C15-N17	-172.946
Glycine	O9-C1	1.353	O9-C1-O8	123.058	N3-C2-C1-O8	19.766
	C1-C2	1.512	C2-C1-O9	111.662	O9-C1-C2-N3	-162.282
	C2-N3	1.455	C2-C1-O8	125.246	O8-C1-O9-H10	1.011
	C1-O8	1.205	N3-C2-C1	110.486	H10-O9-C1-O8	-176.964
UO$_2$-Met (1:1)	O22-U1	2.266	O30-U1-O24	71.779	O22-U1-N2-C3	-173.546
	U1-O20	2.011	O30-U1-O22	128.292	O30-U1-N2-C3	86.421
	U1-O32	2.800	O30-U1-O20	70.016	O24-U1-N6-C5	100.027
	U1-O24	2.270	O30-U1-O32	146.683	N9-C5-N6-C5	-127.278
	U1-O30	2.701	O30-U1-O21	128.292	U1-N6-C5-N4	55.412
	U1-O21	2.009	O30-U1-N6	76.971	C3-N2-U1-O20	131.343
	U1-N2	2.545	O30-U1-N2	128.101	C5-N6-U1-O22	177.443
	U1-N6	2.376	N2-U1-N6	70.928	N2-C3-N8-C12	-179.757
	N2-C3	1.301	N2-U1-O32	73.446	C3-N4-C5-N9	-179.572
	C3-N4	1.430	N2-U1-O20	72.189	N8-C3-N2-U1	176.310
UO$_2$-Met (1:2)	N2-C3	1.298	N26-C21-N20	114.296	N26-C21-N20-U1	143.882
	C3-N4	1.407	N23-C24-N25	123.518	N23-C24-N25-U1	12.991
	C5-N6	1.450	C24-N25-U1	133.597	C21-N20-U1-O42	-95.165
	U1-C6	2.528	C21-N20-U1	124.301	C24-N25-U1-O42	5.503
	U1-N20	2.401	O42-U1-O40	172.640	C5-N6-U1-O25	-165.387
	O42-U1	2.353	N2-U1-N6	65.871	N4-C3-N2-U1	2.180
	N20-C21	1.435	C3-N2-U1	141.030	U1-N6-C5-N4	-14.173
UO$_2$-Met-Gly (1:1:1)	C6-N7	1.466	N10-C3-N2	110.586	N2-U1-N24-C25	143.078
	C3-N2	1.465	C6-N12-N7	110.444	C16-N10-C3-N5	71.987
	N2-U1	2.387	N2-U1-N7	78.285	C27-O30-U1-N2	-133.837
	U1-N7	2.373	O36-U1-N7	138.546	C3-N2-U1-N24	138.526
	U1-O34	2.255	N2-U1-O30	130.849	N5-C6-N7-U1	-41.924
	U1-O36	2.261	O30-U1-N24	71.570	O30-U1-N24-C25	15.709
	U1-O30	2.222	U1-N24-C25	114.338	U1-N2-C3-N5	-52.113
	U1-N24	2.374	U1-O30-C27	119.978	N7-U1-N2-C3	-8.295

Table 3 and Figure 12 show the geographic distribution of molecular orbital FMO maps of HOMO, LUMO, and energies of the examined ligands and complexes in the ground state. EHOMO's computed values, which describe their ability to donate electrons. ELUMO of the ligands, on the other hand, characterizes its electron affinity. Finally, the computed energy gap, (Eg), computes a compound's reactivity; as the energy gap lowers, the compound's reactivity increases (Table 3). After complexation, the ligand's LUMO values stabilize, resulting in an increase in the electron affinity of the complexes. The molecule's energy gap revealed its chemical stability and electron conductivity, making it the most important determinant in determining its molecular electrical transport. The energy gap (Eg) of the complexes is lower than the ligands, demonstrating the more reactive nature of the complexes. Using B3LYP/6.311G** (d,p) and B3LYP/GEN, the

energies of HOMO and LUMO were utilized to compute the energy gap, ionization energy (I, eV), electron affinity (A, eV), absolute electronegativities, (χ, eV), absolute hardness (η, eV), Absolute softness (σ, eV), global softness (S, eV) chemical potential (P, eV) global electrophilicity (ω, eV), additional electronic charge, ΔN_{max} of the investigated ligands and complexes. The results show that the chemical potential (P) of UO_2-Met (1:1), UO_2-Met (1:2), UO_2-Met-Gly (1:1:1) complexes were more negative than that of the ligands, indicating that they were more reactive. As a result, the complexes' chemical hardness (η) is lower than the ligands, while their chemical softness (S) follows the opposite trend (Table 3). As a result, charge transfer is more easily accomplished in these complexes. Electrostatic potential maintains the variation of electronegativity (χ) values in the complexes for any two molecules where the electron is partially transferred from one of lower to that of higher. The results reveal that when the values decrease, charge transport within these complexes increases. Moreover, the arrangement of the magnitudes P, ω and ΔN show that the complexes is electronically less stable and has a high electrophilicity index and charge transfer ability.

Table 3. Total energy, energy of HOMO and LUMO, energy gap, ionization energy (I, eV), electron affinity (A, eV), absolute electronegativities, (χ, eV), absolute hardness (η, eV), Absolute softness (σ, eV), global softness (S, eV) chemical potential (P, eV) global electrophilicity (ω, eV), additional electronic charge, $\Delta Nmax$, of Metformin, Glycine, UO_2-Met (1:1), UO_2-Met (1:2), UO_2-Met-Gly (1:1:1) using B3LYP/GEN level.

Parameter	Metformin	Glycine	UO_2-Met (1:1)	UO_2-Met (1:2)	UO_2-Met-Gly (1:1:1)
E_T (eV)	-11780	-7742	-37152	-44772	-40764
E_{HOMO} (eV)	-5.6133	-6.6213	-6.7740	-6.1859	-6.6472
E_{LUMO} (eV)	-0.5801	-0.0225	-2.1379	-1.4144	-2.4024
E_g (eV)	5.0332	6.5987	4.6360	4.7715	4.2686
I (eV)	152.7468	180.1762	184.3314	168.3282	152.7469
A (eV)	15.7854	0.612261	58.17568	38.48809	65.37315
χ (eV)	84.2661	90.39421	121.2535	103.4082	123.127
η (eV)	68.4807	89.78195	63.07785	64.92007	57.7539
S (eV)	0.0073	0.00012	0.00025	0.00024	0.0003
σ	0.0146	0.1114	0.1585	0.1540	0.1731
P (eV)	-84.2661	-90.3942	-121.254	-103.408	-123.127
ω (eV)	51.8451	45.5053	116.5418	82.3570	131.2488
$\Delta Nmax$	1.2305	1.0068	1.9222	1.5928	2.13192

In the fields of photoelectronics and laser technology, NLO materials can produce second harmonic generation (SHG). There is no experimental or theoretical research on NLO for the examined ligands and their UO_2(II) complexes in the literature. Because of their potential in optical information processing, optical computing, telecommunications, and optical data storage, NLO materials have created a lot of attention **(Chemia *et al.*, 1987 ;**

Natarajan *et al.,* 2008 ; Bradshow and Andrews 2009). B3LYP/GEN was used to calculate the link between molecular structure and NLO characteristics, as well as the polarizabilities and hyperpolarizabilities of the $UO_2(II)$ complexes investigated. Table 4 shows the total static dipole moment (μ), The magnitude of their dipole moment indicates that all the complexes investigated were polar molecules. The direction of the dipole moment vector can be related to the increase in the dipole moment of the complexes. Therefore, the polarity follows the order UO_2-Met-Gly (1:1:1)>UO_2-Met (1:1)>UO_2-Met (1:2), mean polarizability (<α>), polarizability anisotropy (Δα), and mean first-order hyperpolarizability (<β>) of the $UO_2(II)$ complexes and the ligands. The polarizabilities and first order hyperpolarizabilities were expressed in atomic units (a.u.), and the estimated values were converted to electrostatic units (esu) using a conversion ratio of 0.1482×10^{-24} esu for α and 8.6393×10^{-33} esu for β. In NLO investigations, urea **(Lin *et al.,* 2002)** is a common prototype (β= 0.1947×10^{-30}). Because there weren't any experimental findings of NLO characteristics of the $UO_2(II)$ complexes and the ligands, urea was chosen as reference material in this investigation. One of the most important aspects of the NLO system is the molecule hyperpolarizability (<β>). The $UO_2(II)$ complexes, are 5, 2 and 10 times larger than Urea, respectively, according to the computed (<β>) values. As a result, all the $UO_2(II)$ complexes investigated have significant polarizability and first order hyperpolarizability and were expected to be encouraging applicants for NLO materials.

Table 4. Calculated total static dipole moment (μ), the mean polarizability <α>, anisotropy of the polarizability Δα and the first order hyperpolarizability configuration for Metformin, Glycine, UO_2-Met (1:1), UO_2-Met (1:2) and UO_2-Met-Gly (1:1:1) using B3LYP/GEN level.

Parameter	Metformin	Glycine	UO_2-Met (1:1)	UO_2-Met (1:2)	UO_2-Met-Gly (1:1:1)
μ, D	2.3180	1.9728	5.7609	2.8033	12.5945
XX	-41.4634	-22.9522	-122.6491	-131.08	-132.0041
YY	-52.3761	-32.7135	-112.0094	-127.568	-144.7357
ZZ	-59.9596	-30.2530	-130.3503	-186.8575	-149.9874
XY	-4.8541	1.1073	11.9341	12.49	-20.0726
XZ	2.5389	-3.1953	2.4517	8.7789	16.2933
YZ	-0.6484	0.1798	-4.2570	18.9841	9.6922
<α>	-0.7597×10^{-23}	-0.4244×10^{-23}	-1.8938×10^{-23}	-2.2008×10^{-23}	-2.1080×10^{-23}
Δα	2.38×10^{-24}	1.30314×10^{-24}	1.1413×10^{-24}	8.5384×10^{-24}	2.3737×10^{-24}
XXX	23.757	13.4303	55.2674	30.2034	-40.252
XXY	-6.3675	2.5148	1.1526	-5.1711	-93.1754
XYY	-5.6513	-5.6260	-7.4722	0.9466	6.6998
YYY	-2.1859	-1.7556	54.3485	17.9038	-101.9868
XXZ	9.4283	6.0777	7.9699	-2.0864	38.5438
XYZ	-5.2122	-0.9032	14.6836	-11.0773	16.9387
YYZ	4.8357	-0.1428	-20.4180	8.1485	26.8208
XZZ	-5.0165	4.4555	43.9796	8.0917	5.0013
YZZ	-0.6098	0.0954	-8.4111	-11.7322	-6.3833
ZZZ	0.0271	1.5409	-18.1921	30.1714	32.5327
<β>	0.1851×10^{-30}	0.1243×10^{-30}	0.9296×10^{-30}	0.4615×10^{-30}	1.9514×10^{-30}

	HOMO	**LUMO**	

Metfor min

Glycin e

UO$_2$- Met (1:1)

UO$_2$- Met (1:2)

UO$_2$- Met- Gly (1:1:1)

LUMO
(Fixed excited state)
E$_{LUMO}$ = -0.5801 eV
E$_{gap}$ = 5.0332 eV
E$_{HOMO}$ = -5.6133 eV
HOMO
(Ground state)

LUMO
(Fixed excited state)
E$_{LUMO}$ = -0.0225 eV
E$_{gap}$ = 6.5987 eV
E$_{HOMO}$ = -6.6213 eV
HOMO
(Ground state)

LUMO
(Fixed excited state)
E$_{LUMO}$ = -2.1379 eV
E$_{gap}$ = 4.6360 eV
E$_{HOMO}$ = -6.7740 eV
HOMO
(Ground state)

LUMO
(Fixed excited state)
E$_{LUMO}$ = -1.4144 eV
E$_{gap}$ = 4.7715 eV
E$_{HOMO}$ = -6.1859 eV
HOMO
(Ground state)

LUMO
(Fixed excited state)
E$_{LUMO}$ = -2.4024 eV
E$_{gap}$ = 4.2686 eV
E$_{HOMO}$ = -6.6472 eV
HOMO
(Ground state)

Fig 12. HOMO and LUMO molecular orbital maps of the ligands and complexes using B3LYP/GEN level.

The charge transfer and natural charges on active sites of the complexes can be efficient in terms of electrophilic and nucleophilic force, as well as hydrogen bonding interactions in any molecular approach (**Murray and Sen, 1996).** The order of rising potential following the sequence: red < orange < yellow < green < blue, red < orange < yellow < green < blue (**Politzer and Murray 2002 ; Sajan *et al.,* 2011**). The optimal structure was analyzed using the computed 3D MEP maps of the complexes and the ligands in the explored complexes, as illustrated in Figure 13. The results demonstrate that the negative

area (red) of the ligands is primarily on the O and N atomic sites, which is due to the contribution of lone-pair electrons from oxygen and nitrogen atoms. The positive (blue) potential sites, on the other hand, are found surrounding the hydrogen and carbon atoms. The potential of the other carbon atoms appears to be zero. The significantly negative potential is over the oxygen atoms and nitrogen of the ligands in MEP maps of UO2(II) complexes, Figure 13, while the largely positive regions are over the hydrogen atoms and the remaining carbon atoms appear to have zero potential. The electrophilic attack will affect the fragment of the molecule that has a negative electrostatic potential, the more negative the electrostatic potential, the better the affinity for the electrophilic attack.
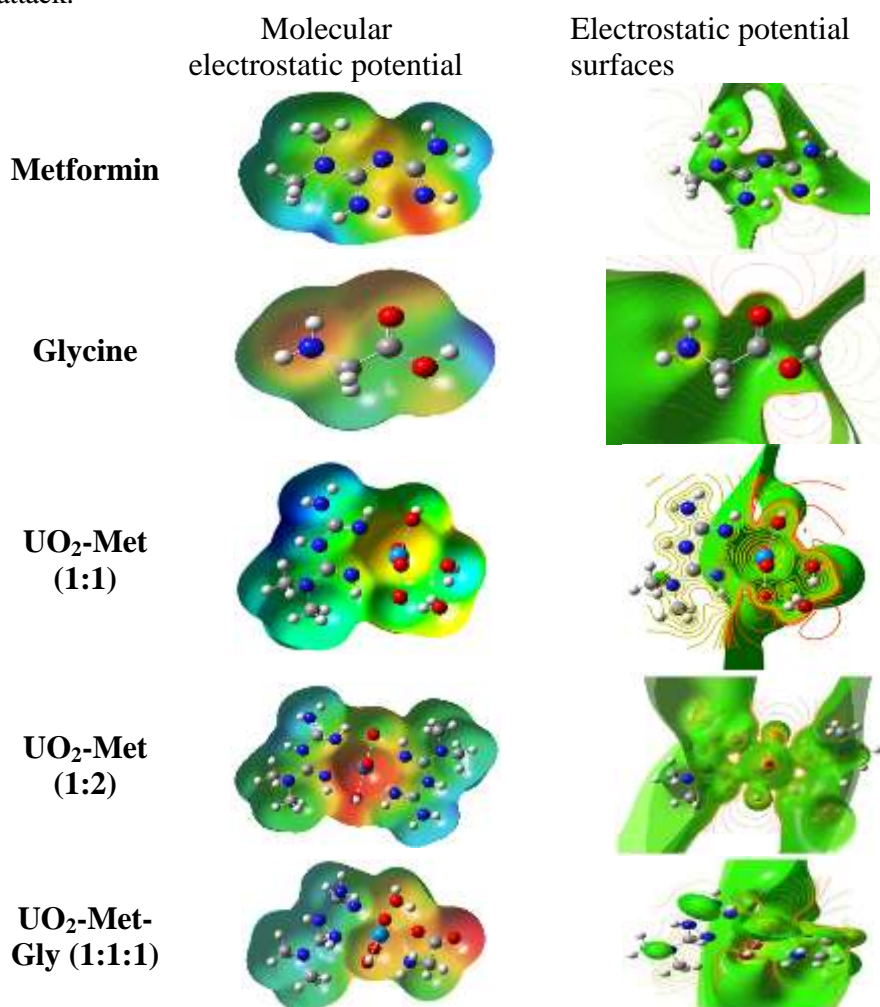
Fig 13. Electrostatic potential & molecular electrostatic potential surfaces of the ligands and the complexes using B3LYP/GEN level.

CONCLUSION

In the present work, a simple and efficient method for the preparation of UO_2-Met (1:1), UO_2-Met (1:2), and UO_2-Met-Gly (1:1:1) complexes via the reflux method that involves Metformin and Glycine as ligands and the appropriate uranyl sulfate as metal ions was developed. UO_2-Met (1:1), UO_2-Met (1:2), and UO_2-Met-Gly (1:1:1) complexes have been fully described using various analytical tools. The metal complexes were also subjected to elemental analysis. The mass spectra of the complexes display a molecular ion peak at m/z = 432, 652, and 523 respectively, which agree with the empirical formula as shown in the elemental analysis. The ligands and their complexes molecular structures were optimized using the SDD basis sets. The compounds can be simply polarized and display significant NLO characteristics, as seen by the confine HOMO-LUMO energy gap. The chelates polarizability and hyperpolarizabilities mean that they are efficient candidate for NLO material. The UO_2-Met (1:2) complex has higher energy than that of the UO_2-Met (1:1) and UO_2-Met-Gly (1:1:1) complexes. This gives further confirmation for the formation of the more stable UO_2-Met (1:2) complex.

REFERENCES

Abd-El Hafeez, S.I. ; N.E. Eleraky ; E. Hafez and S.A. Abouelmagd (2022): Design and optimization of Metformin hydrophobic ion pairs for efficient encapsulation in polymeric drug carriers. Sci. Rep., 12(1):1–14.

Abdel-Ghani, N.T. and O.E. Sherif (1989): Potentiometric, conductimetric, spectrometric, thermogravimetric, and magnetic studies of lanthanum complexes with some symmetric 1,5-diaryl-3-cyanoformazans. Thermochim. Acta., 156(1):69–83.

Abdel-Latif, S.A. ; H.B. Hassib and Y.M. Issa (2007): Studies on some salicylaldehyde Schiff base derivatives and their complexes with Cr(III), Mn(II), Fe(III), Ni(II) and Cu(II). Spectrochim. Acta. A., 67(3–4):950–957.

Avci, D. ; A. Basoglu and Y. Atalay (2010): Ab initio HF and DFT calculations on an organic non-linear optical material. Struct. Chem., 21 (1): 213-219.

Avci, D.(2011): Second and third-order nonlinear optical properties and molecular parameters of azo chromophores: Semiempirical analysis. Spectrochimica Acta Part A: Molecular and Biomolecular Spectroscopy, 82(1):37-43.

Babij, N.R. ; E.O. McCusker ; G.T. Whiteker ; B. Canturk ; N. Choy. and L.C. Creemer (2016): NMR chemical shifts of trace impurities: industrially preferred solvents used in process and green chemistry. Org. Process Res. Dev., 20(3):661–667.

Bentefrit, F. ; G. Morgant ; B. Viossat ; S. Leonce ; N. Guilbaud and A. Pierre (1997): Synthesis and antitumor activity of the Metformin platinum (IV) complex. Crystal structure of the tetrachloro (Metformin)platinum (IV) dimethylsulfoxide solvate. J. Inorg. Biochem., 68(1):53–9.

Bradshow, D.S. and D.L. Andrews (2009): Quantum channels in nonlinear optical processes. J. Non-linear Opt. Phys. Matter., 18: 285-299.

Chemia, D.S. and J. Zyss (1987): Nonlinear Optical Properties of Organic Molecules and Crystals, Academic Press, Orlando, FL, USA.

Chen, C. ; J. Fang and C. Xu (2021): Ultrasonication Mediated Fabrication of Glycine Coated Gadolinium Oxide Nanoparticles as MRI Contrast Agents. J. Clust. Sci., 32(3):773–8.

Dennington, R. ; T. Keith and J. Millam (2009): Gauss View, Version 5. Semichem Inc., Shawnee Mission. 16-R. Dennington, T. Keith, J. Millam, Gauss View, Version 5, K.S. Shawnee Mission, Semichem. Inc.

Frisch, M.J. ; G.W. Trucks ; H.B. Schlegel ; G.E. Scuseria ; M.A. Robb ; J.R. Cheeseman ; G. Scalmani ; V. Barone ; B. Mennucci ; G.A. Petersson ; H. Nakatsuji ; M. Caricato ; X. Li ; H.P. Hratchian ; A.F. Izmaylov ; J. Bloino ; G. Zheng ; J.L. Sonnenberg ; M. Hada ; M. Ehara ; K. Toyota ; R. Fukuda ; J. Hasegawa ; M. Ishida ; T. Nakajima ; Y. Honda ; O. Kitao ; H. Nakai ; T. Vreven ; J.A. Montgomery Jr. ; J.E. Peralta ; F. Ogliaro ; M. Bearpark ; J.J. Heyd ; E. Brothers ; K.N. Kudin ; V.N. Staroverov ; R. Kobayashi ; J. Normand ; K. Raghavachari ; A. Rendell ; J.C. Burant ; S.S. Iyengar ; J. Tomasi ; M. Cossi ; N. Rega ; J.M. Millam ; M. Klene ; J.E. Knox ; J.B. Cross ; V. Bakken ; C. Adamo ; J. Jaramillo ; R. Gomperts ; R.E. Stratmann ; O. Yazyev ; A.J. Austin ; R. Cammi ; C. Pomelli ; J.W. Ochterski ; R.L. Martin ; K. Morokuma ; V.G. Zakrzewski ; G.A. Voth ; P. Salvador ; J.J. Dannenberg ; S. Dapprich ; A.D. Daniels ; Ö. Farkas ; J.B. Foresman ; J.V. Ortiz ; J. Cioslowski and D.J.

Fox,(2010) Gaussian 09, Revision B.01. Gaussian Inc., Wallingford.

Grzybowska, M. ; J. Bober and M. Olszewska (2011): Metformina – mechanizmy działania i zastosowanie w terapii cukrzycy typu 2[i][/i]. Postepy Hig Med Dosw., 65: 277–285.

Heidari, M. ; A. Sedrpoushan and F. Mohannazadeh (2017): Selective oxidation of benzylic C-H using nanoscale graphene oxide as highly efficient carbocatalyst: Direct synthesis of terephthalic acid. Org. Process Res. Dev., 21(4):641–647.

Inzucchi, S.E. ; R.M. Bergenstal ; J.B. Buse ; M. Diamant ; E. Ferrannini and M. Nauck (2012): Management of hyperglycaemia in type 2 diabetes: A patient-centered approach. Position statement of the American Diabetes Association (ADA) and the European Association For The Study Of Diabetes (EASD). Diabetologia., 55(6):1577–96.

Krishan, B. ; M. Tawkir and S.A. Iqbal (2012): Synthesis, spectral characterization, magnetic moment, mass, X-Ray diffraction, and kinetic (TGA) studies of cr(III) complex with Metformin: An oral antidiabetic drug. Orient. J. Chem., 28(4): 1883-1888.

Lemoine, P. ; M. Chiadmi ; V. Bissery and A. Tomas (1996): Viossat B. Les composés de la Metformine avec les ions Co(II), Cu(II) et Ni(II). Acta Crystallogr C., 52(6):1430–6.

Lin, Y.Y. ; N.P. Rajesh ; P.S. Raghavan ; P. Ramasamy and Y.C. Huang (2002): Crystal growth of two-component new novel organic NLO crystals. Mater. Lett., 56: 1074-1077.

Mahmoud, M.A. ; E.T. Abdel-Salam ; N.F. Abdel Aal ; Z.M. Showery and SA. Sallam (2019): Dy(III) complexes of Metformin Schiff-bases as glucose probe: synthesis, spectral, and thermal properties. J. Coord. Chem., 72(4):749–69.

Matthaei, S. and H. Greten (1991): Evidence that Metformin ameliorates cellular insulin-resistance by potentiating insulin-induced translocation of glucose transporters to the plasma membrane. Diabete Metab.,17(1 - 2):150–158.

Murray, J.S. and K. Sen (1996): Molecular Electrostatic Potential Concepts and Applications, Elsevier, Amsterdam, The Netherlands.

Natarajan, S. ; G. Shanmugam and S.A.M.B. Dhas (2008): Growth and characterization of a new semi organic NLO material: L-tyrosine hydrochloride. Cryst. Res. Technol., 43: 561-564.

Olar, R. ; M. Badea ; E. Cristurean ; V. Lazar ; R Cernat and C. Balotescu (2005): Thermal behavior, spectroscopic and biological characterization of Co(II), Zn(II), Pd(II) and Pt(II) complexes with N,N-dimethylbiguanide. J. Therm. Anal. Calorim., 80(2):451–455.

Panda, B.P. ; R. Krishnamoorthy ; N.K.H. Shivashekaregowda and S. Patnaik (2018): Influence of poloxamer 188 on design and development of second generation PLGA nanocrystals of Metformin hydrochloride. Nano Biomed Eng., 10(4):334–343.

Politzer, P. and J.S. Murray (2002): The fundamental nature and role of the electrostatic potential in atoms and molecules. Theor. Chem. Acc., 108: 134-142.

Refat, M.S. ; F.M. Al-Azab ; H.M.A. Al-Maydama ; R.R. Amin ; Y.M.S. Jamil and M.I. Kobeasy (2015): Synthesis, spectroscopic and antimicrobial studies of La(III), Ce(III), Sm(III) and Y(III) Metformin HCl chelates. Spectrochim Acta A Mol Biomol Spectrosc., 142: 392–404.

Robert, H.M. ; D. Usha ; M. Amalanathan ; R.R.J. Geetha and M.S.M. Mary (2020): Spectroscopic (IR, Raman, UV, NMR) characterization and investigation of reactive properties of pyrazine-2-carboxamide by anti-bacterial, anti-mycobacterial, Fukui function, molecular docking and DFT calculations. Chemical Data Collections., p 30.

Sajan, D. ; L. Joseph ; N. Vijayan and M. Karabacak(2011): Natural bond orbital analysis, electronic structure, non-linear properties and vibrational spectral analysis of l-histidinium bromide monohydrate: A density functional theory. Spectrochim. Acta, Part A., 81: 85-98.

Scarpello, J.H.B. and H.C.S. Howlett (2008): Metformin therapy and clinical uses. Diab Vasc. Dis. Res., 5(3):157–67.

Shahabadi, N. and L. Heidari (2012): Binding studies of the antidiabetic drug, Metformin to calf thymus DNA using multispectroscopic methods. Spectrochim. Acta-part A Mol Biomol Spectrosc., 97:406–4010.

Viossat, B. ; A. Tomas and N.H. Dung (1995): L'hydrogénocarbonate de Bis (N,N-diméthylbiguanide) Cuivre(II), [Cu(C4H11N5)2]2HCO3. Acta Crystallogr C., 51(2):213–5.

Wang, Y.W. ; S.J. He ; X. Feng ; J. Cheng ; Y.T. Luo and L. Tian (2017): Metformin: A review of its potential indications. Drug Des. Devel. Ther. , 11:2421–2429.

Zhu, M. ; L. Lu ; P. Yang and X. Jin (2002a): Bis(1,1-dimethylbiguanido) copper (II) octahydrate. Acta Crystallogr Sect E Struct Rep Online., 58(5):m217–9.

Zhu, M. ; L. Lu ; X. Jin and P. Yang (2002b): Trichloro (1, 1-dimethylbiguanidium-κN3) zinc (II). Acta Crystallogr C. 2002; 58(3):m158–9.

التحضير والتوصيف والدراسات النظرية DFT للميتفورمين مختلط مع الجلايسين ومتراكباتهم مع أيونات اليورانيل.

محمد مجدي درويش ، سمير عبداللطيف ، عادل محمد

قسم الكيمياء – كلية العلوم – جامعة حلوان

تم تحضير متراكبات اليورانيوم (II) UO2 مع ميتفورمين ليجند (1،1–ثنائي ميثيل بيجوانيد) (Met) و (Gly) Glycine كليجند مختلط (حمض أمينو أسيتيك) وتوصيفها باستخدام تقنيات مختلفة. كما أجريت دراسات نظرية (نظرية الكثافة الوظيفية ، DFT) لدعم النتائج التجريبية المقابلة. تم إجراء الحسابات الحسابية باستخدام مستوى نظرية GEN / DFT للمعدن. تمت دراسة طبيعة التفاعل بين أيونات المعادن والرابط ، والاستقرار الجزيئي ، وقوة الرابطة باستخدام حسابات DFT التي تستخدم التحليل المداري للرابطة الطبيعية (NBO). تم دعم انتقائية التفاعل من خلال الحسابات النظرية على مستوى DFT. تم إجراء التركيب الجزيئي الأمثل ومدار الرابطة الطبيعية (NBO) بواسطة نظرية الكثافة الوظيفية (DFT) باستخدام B3LYP/GEN لليجند .